



Numerical Simulation of Hybrid Platform Supply Vessel (PSV) Fuel Consumption for the Pre-Salt Layer in Brazil

Kazuo Nishimoto^{1(✉)}, Claudio M. P. Sampaio¹, Rodrigo J. Vale¹,
and Felipe Ruggeri²

¹ Dept Engenharia Naval e Oceânica,
University of São Paulo (USP), São Paulo, Brazil
knishimo@usp.br

² Argonáutica Engenharia e Pesquisas, São Paulo, Brazil

Abstract. The new regulations regarding ship emissions based on IMO regulations combined to the high fuel prices require the application of new technologies to improve ship efficiency and to reduce the CO₂, NO_x, SO_x and BC emissions. The application of LNG as fuel and battery packs to improve the conventional engines performance are already a reality in offshore supply vessels (OSV) around the world. However, the reduction in OPEX and payback time of the additional investment is very dependent of the ship operational profile, which are related to the FPSOs and port facilities particularities in Brazil. In order to estimate the advantages of these technologies in the PSV overall performance several different simulators regarding DP operation, sailing, waiting and anchored mode are combined to obtain a digital twin of the vessel. These simulators are combined to the real data monitored from the ships regarding ship speed, position and heading collected in Brazil based on AIS/AIS-Sat database. This database is combined to the environmental conditions regarding wave, current and wind obtained based on global numerical models to provide the environmental loads acting in the ship during the different stages of the operation. The DP simulations are performed applying a thrust allocation algorithm, the calm water resistance is obtained based on regression models and the added resistance due to waves are computed based on strip theory. The forces are converted into electric load by considering the propeller, generators, switchboard, electric drive and engine efficiency curves combined to a power management system (PMS) algorithm, which balance the loads in the engines according to the operational mode. The baseline for comparison is the current PSV without dual-fuel engines or battery pack.

Keywords: Platform Supply Vessel · Dual fuel · Ship efficiency

1 Introduction

The pre-salt support operations are becoming more and more frequent in Brazil due to the exploration of the Pre-salt layer oil reservoir. In order to reduce the ship emissions and fuel consumption a basic comprehension of the operational profile of these vessels,

as the efficiency and possible modifications of the operational profile is required. This task may be performed using a numerical simulator to reproduce the vessel operation.

The studied ship was defined as a PSV 4500 with the main characteristics shown in Table 1, which was established based on similar vessels operating in the pre-salt of Brazil. The selected vessel has 4 main generators that provides energy to two bow tunnel thrusters and one retractable azimuthal thruster in bow that provide control in the fore region while there are two azimuthal thruster located in the stern region used for both propulsion and station keeping.

Table 1. Ship properties and power characteristics of PSV4500.

Dimension	Value		Equipment	Power	
LOA	86.8	m	Main generator	6809	kW
Beam	18.8	m	(4 x Gen)	1702	kW
Depth	7.96	m	Main prop power	4319	kW
Draft	6.52	m	2 x Azimuth Nozzle	2159	kW
DWT	7500	ton	Bow thruster	2275	kW
Speed	14.2	kn	(2 x Tunnel +	813	kW
Displacement	7475	ton	+ 1 retractable)	650	kW

2 Environmental Conditions

2.1 Wave Conditions

The wave conditions were post-processed based on the several results from Wave Watch III (WW3) model run directly by NOAA (National Oceanic and Atmospheric Administration) and provided through a specific FTP. The numerical results are available in several points in the Brazilian coast (Fig. 1) but the most important ones are located near Santos and Campos Basins, since there are a large number of oil platforms in these regions. Besides, Açú port (in white) was selected as base port for PSV simulations because its very near location to a large cluster of oil platforms.

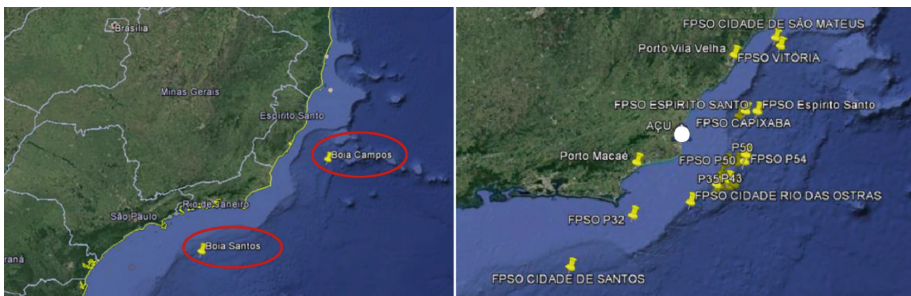


Fig. 1. Points provided by NOAA environmental conditions, buoys (left) and oil platforms located in Santos and Campos Basin (yellow) and Açú port (white) (right).

The results regarding the wave conditions were download during the period between August 1st, 2015 to January 1st, 2016 considering the simulated sea state with a time sample of 1 h, providing 12473 records. For each sea state partition the significant wave height is provided, as the peak period, the peak wave direction and the directional spread. For each partition the numerical model also provides the fraction of this wave component that is generated locally (sea) or propagated from other locations (swell).

The several files were post-processed providing the wave record for Campos Basin shown in Fig. 2 and Fig. 3, regarding the significant wave height and peak period. In order to provide a comprehension between these wave conditions the results are presented for sea and swell conditions considering the two most energetic components among the several partitions.

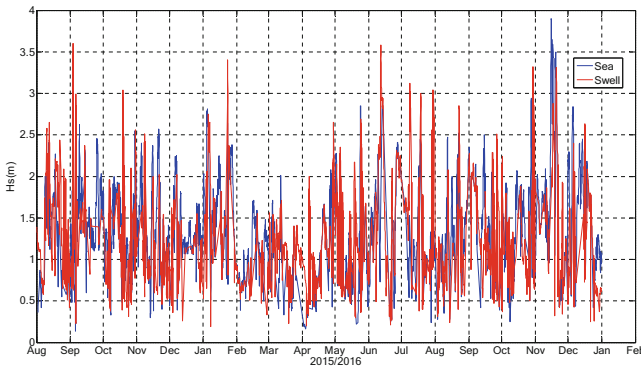


Fig. 2. Time series of significant wave height in the period between August 1st, 2015 and January 1st, 2016 for the Campos Basin point.

It can be observed significant wave heights over 3.5 m and peak periods up to 18 s, which may induce large vessel motions during the operations. Since the Campos Basin is located very far from the coast, the wind fetch is almost unlimited, therefore the locally generated waves (sea) may reach large significant wave heights and peak periods up to 12 s, which is uncommon compared to the sheltered locations (ex: ports and harbors).

It can be verified that sea conditions generated by the local winds are provided most from the northeast direction with peak periods usually below 7 s, although in almost 2% reaches 8 s. The significant wave height generated by the local wind reaches up to 2.0 m most of the times but for about 5% of the time the wave height reaches 2.5 m and for less than 1%, 4.0 m height. On the other hand, the swell wave conditions reach the Campos Basin from the east and south directions, the first one with more occurrences but the second one with more intensity in terms of significant wave height. The waves coming from the east direction usually reach up to 2.0 m–2.5 m with peak periods below 10 s while the waves from the south reach up to 3.5 m and 16 s, which are long wave conditions (~ 400 m wavelength).

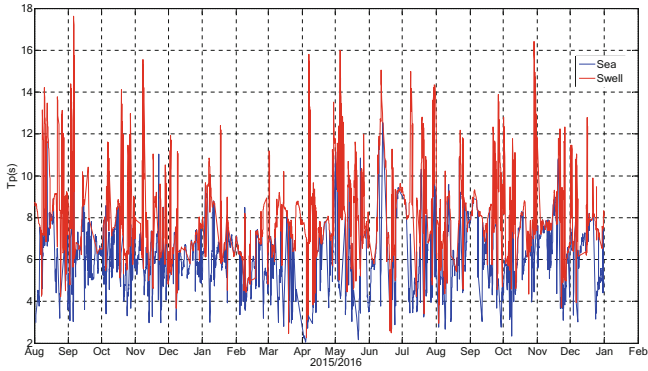


Fig. 3. Time series of peak period in the period between August 1st, 2015 and January 1st, 2016 for the Campos Basin point.

2.2 Wind Conditions

The wind conditions obtained from NOAA data for Campos Basin are shown, in terms of average intensity and direction, in Fig. 4 where wind speeds up to 30 knots can be verified, although the average speed during the year is about 15 knots.

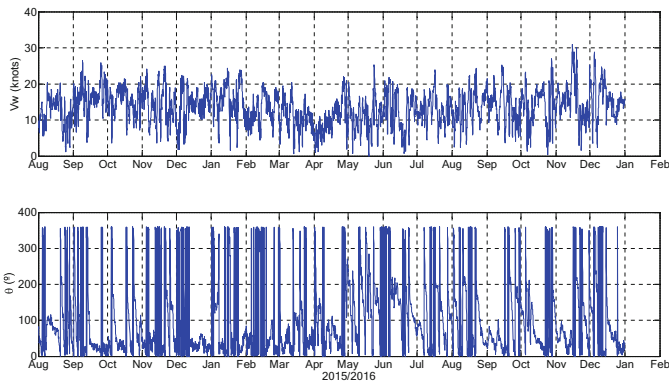


Fig. 4. Time series of wind speed and direction between August 1st, 2015 and January 1st, 2016 for the Campos Basin point.

2.3 Current Conditions

Since the current conditions were not available in NOAA data, these data were obtained from HYCOM project (HYCOM 2017). The data was extracted from the webservice available in the project website and collected considering all water depth layers from the sea bottom to the sea surface. However, since for the simulation only the current acting on the ship's hull is of interest, the mean values of the current were computed between the mean sea surface and 6.0 m water depth (ship's draft).

The time series of current intensity and direction is illustrated in Fig. 5, where the current direction is conventionally defined as *going to*. It can be verified that current intensity reaches up to 1.5 knots in extreme conditions, although most of the time the values are below 0.8 knots. It can also be observed that the current direction is widely spread in the south sector with predominant direction as southwest.

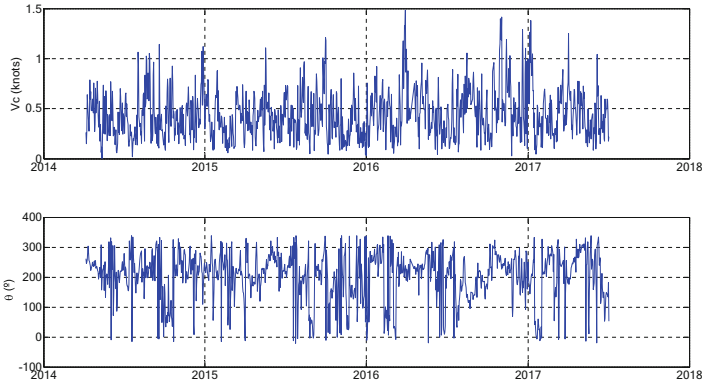


Fig. 5. Time series of current speed and direction between August 1st, 2015 and July 1st, 2017 for the Campos Basin point.

3 Mathematical Models

Since the PSV operational activities change appreciably, several different models were combined to provide an integrated simulator. The DP model computation is based on a quasi-static approach where the total thrust required in the fore and stern regions are computed in terms of time average loads that is, although an entire year of environmental records on each set of wind, current and sea state conditions were used, only the average thrust was computed. In order to control the degrees of freedom in the plane (surge, sway and yaw), the environmental loads considered into the analysis are wind, current, wave mean drift and wave-drift damping loads.

The wind and current loads are computed based on values presented in the literature (Fossen and Perez 2009) and/or based on CFD (Computational Fluid Dynamics) simulations. Other additional sources that could be used are the experimental results published by (Blendermann 1994).

The wave mean drift are computed using the potential flow solver WAMIT® while the wave drift damping loads are obtained based on the approximation proposed by Aranha (Aranha 1994). Since most of these operations are performed in close proximity to a FPSO (Floating Production Storage & Offloading Unit), the correct approach would be to take into account the shadow effects imposed by the unit in terms of wind, current and waves. However, in this simplified version these interactions was not considered.

The several models are integrated to estimate the required thrust that must be provided by the propulsion system in order to obtain the pre-established performance.

It shall be highlighted that in the simulations the ship’s behavior is known through the track records, allowing the characterization of engine loads for the computation of the desired performance.

3.1 Conversion from Required Thrust into Engine Load and Fuel Consumption

The diesel-electric system is modeled considering engines, generators, propellers, switchboards, transformers and electric drives according to available manufacturers’ specification and guidelines. The modeled arrangement is depicted in Fig. 6 with its various components, the electric system distributed into two switchboards that can be connect by a tie.

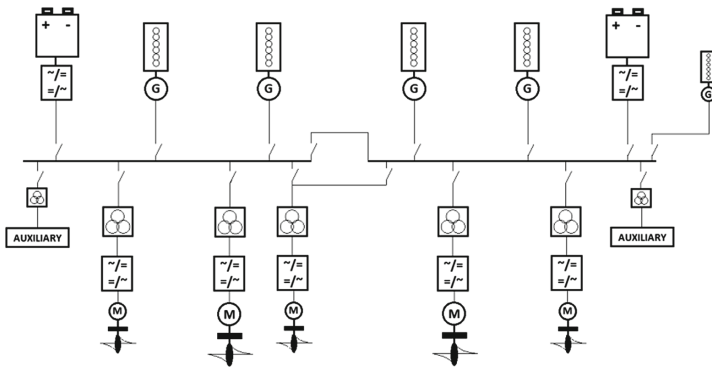


Fig. 6. PSV diesel-electric configuration.

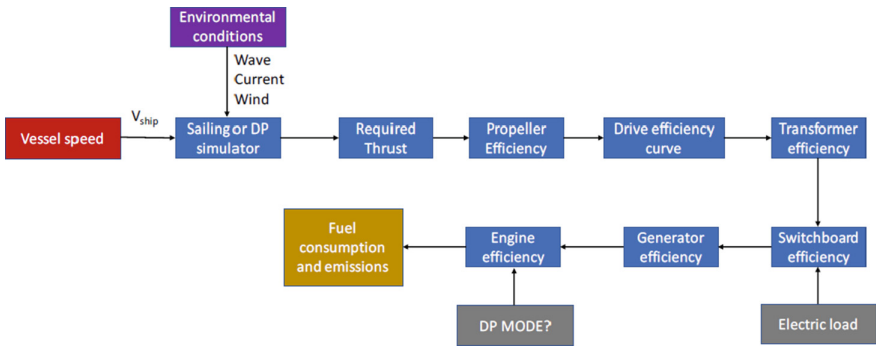


Fig. 7. Blocks diagram of the simulator.

The simulator’s diagram is sketched in Fig. 7, where it can be observed that the vessel speed and the environmental conditions are the input information for the whole computation.

The generators efficiency curve is based on manufacturers’ data, is defined as the ratio between power-out and power-in (Vasques (2014)) and it is a function of power-in, as shown in Fig. 8. It can be seen that the curve is almost flat for power levels above 1000 kW with an efficiency around 97%. On the other side, the generator efficiency reduces appreciably for power levels below 400 kW achieving 87% for powers below 50 kW.

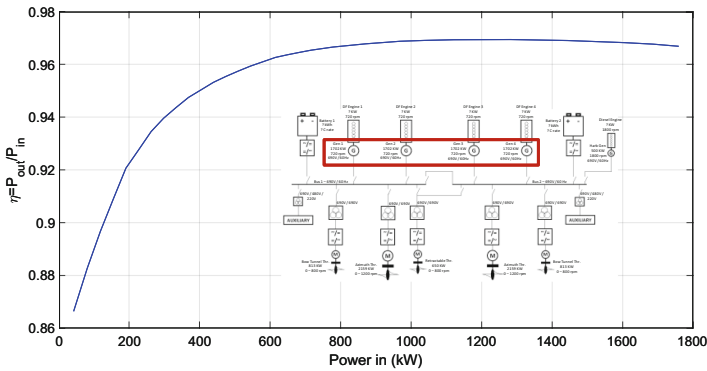


Fig. 8. Generators efficiency curves.

The switchboard and transformer efficiencies are also defined as ratios of power-out and power-in, however, as efficiency variation is low, these efficiencies were assumed constant at 99.5% and 98.5%, respectively. The electric drive efficiency curve has similar characteristics as the other devices as shown in Fig. 9. Based on manufacturer’s catalogue data, its efficiency is function of rotation speed over rated speed. It can be observed that its maximum efficiency is about 90% for rates above 60%, on the other hand, for low rates, the efficiency rapidly falls, an aspect that should be carefully evaluated.

The rotation is computed based on propeller-hull integration assuming modified B-Troost curves that include the nozzle effect (Carlton 1994), this effect increasing the bollard pull thrust at one hand, at the other reducing the propeller efficiency for high advance coefficients. The K_T and K_Q coefficients and the propeller efficiency (η) are defined, respectively, by Eqs. (1), (2) and (3), where T is the propeller thrust; Q , propeller torque; ρ , salt water density; D , propeller diameter and J , the advance coefficient.

$$K_T = \frac{T}{\rho n^2 D^4} \tag{1}$$

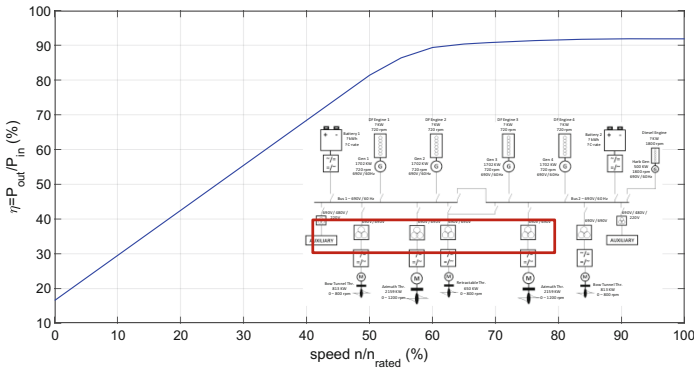


Fig. 9. Electric drive efficiency as function of the rate of speed rate per rated speed.

$$K_Q = \frac{Q}{\rho n^2 D^5} \tag{2}$$

$$\eta = \frac{J K_T}{2\pi K_Q} \tag{3}$$

The propellers characteristics were obtained from similar ships and manufacturers general specifications (Rolls Royce 2014) and are summarized in Table 2. It should be remarked that the azimuthal propellers have controllable pitch, thus the efficiency can be optimized according to the required thrust and rotation.

Table 2. Propellers properties (Blade number = 4 and $A_b/A_0 = 0.55$).

Propeller	Bollard pull (kN)	Diameter (m)	Power (kW)	Maximum rotation (rpm)
Stern azimuth 1	450	2.8	2159	1200
Stern azimuth 2	450	2.8	2159	1200
Bow tunnel 1	150	2.0	813	800
Bow tunnel 2	150	2.0	813	800
Bow azimuth	100	2.0	600	600

An example of conventional propeller diagram (K_T , K_Q and η curves) with nozzle is shown in Fig. 10 for different pitch/diameter (P/D) ratios. However, from the simulation point of view, it is more convenient to obtain a direct relation between propeller thrust and torque, as torque can be converted to required propeller power by Eq. (4), with the ratio between torque and thrust given by expression (5).

$$P = 2\pi nQ \tag{4}$$

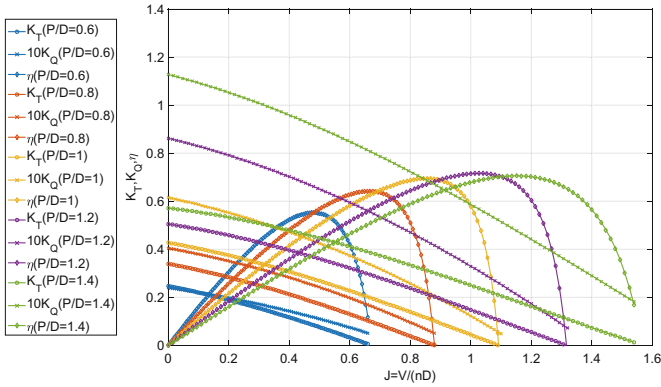


Fig. 10. K_T , K_Q and η curves for PSV propeller.

$$\frac{K_Q}{K_T} = \frac{Q}{TD} \tag{5}$$

The fuel consumption is obtained based on manufacturers’ specific fuel oil consumption (SFOC) of the power output curve of the engine, as depicted in Fig. 11 for diesel and gas engine. Besides, in natural gas mode, dual-fuel engines require a pilot diesel fuel for the beginning of the combustion process, this portion also included in the graph. It can be observed that the SFOC is appreciably higher for loads below 1000 kW.

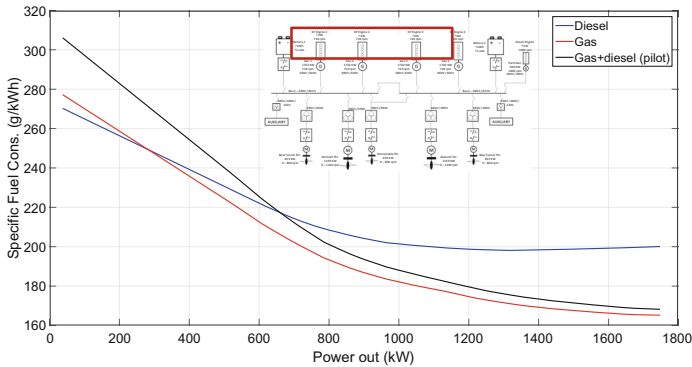


Fig. 11. SFOC curves as function of the power-out.

Since the PSV has more than a single engine, the SFOC of several engines shall be combined to provide the minimum SFOC for the total required ship's load. Since the SFOC is higher at smaller loads for each individual engine, the total SFOC curve has several jumps (Kjølberg (2015)). In practice, there are several different ways to distribute the engine loads to obtain the required power but, in order to provide a more generic simulator, a non-linear optimization problem was solved where the fuel consumption is minimized, as defined by Eq. (6), with SFOC changing according to the engine load x_e . Moreover, the total required power, P_{Req} provided by the engines is defined by constraint (7), each individual engine load limited to its maximum power, given by constraint (8).

$$CT = \sum_{e=1}^{Ne} SFOC(x_e) x_e \quad (6)$$

$$\sum_{e=1}^{Ne} x_e = P_{Req} \quad (7)$$

$$x_e \leq P_{Maxe}, e = 1, 2, \dots, Ne \quad (8)$$

Table 3. Emission factors for different fuels.

Emissions (g/kg fuel)		
Components	Diesel	Gas
CO2	3200	2700
CH4	0.3	31.2
NOX	60	13.7
SOX	10	0.6
BC	0.3	0.03
CO	10	10

Finally, the ship emissions are computed according to conversion factors presented in Table 3 (Stenersen and Thonstad (2017), IPCC (2013), etc.), where they are represented as ratios of emission mass per fuel mass for CO2, CH4, NOX, SOX, black carbon and CO constituents.

4 Environmental Loads

The interactions between vessel and wind, current and waves shall be computed for the evaluation of the required thrust and later evaluation of the demanded electric power and engine loads at the different operational conditions. It is important to highlight that the main difference between DP and navigation modes is the forward speed, which is appreciably higher for the last one.

4.1 Wind Loads

The wind loads are computed based on the coefficients presented by Fossen and Perez (2009) with the longitudinal, transversal and moment loads computed based on Eqs. (7), (8) and (9). In this equations $A_{Frontal}$ is the projected frontal area; $A_{Lateral}$, the projected lateral area; $C_{WX}(\theta_W)$, $C_{WY}(\theta_W)$ and $C_{WM}(\theta_W)$, the wind coefficients; θ_W , the wind incidence angle (measured from the bow in counterclockwise direction); U_W , the wind speed and ρ_{air} , the air density. The windage area is calculated based on the ship’s profile, respectively, 550 m² and 180 m² for lateral and frontal areas. The wind load coefficients are shown in Fig. 12.

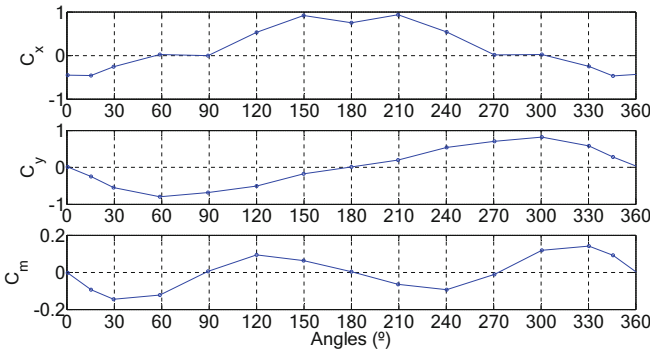


Fig. 12. Wind coefficients: Top C_{WX} ($= C_x$); middle, C_{WY} ($= C_y$) and down, C_{WM} ($= C_m$) – (Fossen and Perez (2009)).

$$F_{Wu}(\theta_W) = \frac{1}{2} \rho_{air} A_{Frontal} C_{WX}(\theta_W) U_W^2 \tag{9}$$

$$F_{Wv}(\theta_W) = \frac{1}{2} \rho_{air} A_{Lateral} C_{WY}(\theta_W) U_W^2 \tag{10}$$

$$M_{Wz}(\theta_W) = \frac{1}{2} \rho_{air} A_{Frontal} L_{PP} C_{WM}(\theta_W) U_W^2 \tag{11}$$

4.2 Current Loads

The current loads are computed analogously to the wind ones by applying Eqs. (10), (11) and (12), where U_C is the current velocity; θ_C , the current incidence angle and $C_{CX}(\theta_C)$, $C_{CY}(\theta_C)$ and $C_{CM}(\theta_C)$, the current coefficients, as shown in Fig. 13.

$$F_{Cu}(\theta_C) = \frac{1}{2} \rho_{water} B T C_{CX}(\theta_C) U_C^2 \tag{12}$$

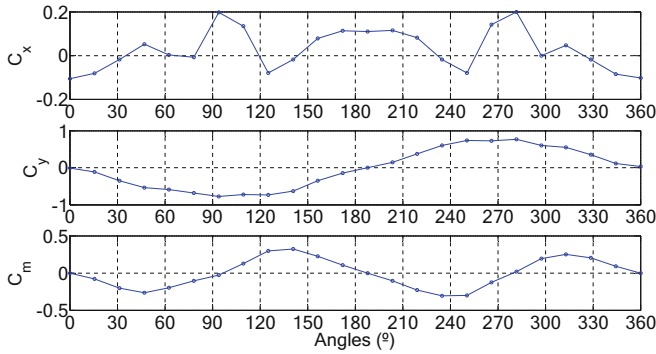


Fig. 13. Current coefficients: Top, C_{CX} ($= C_x$); middle, C_{CY} ($= C_y$) and down, C_{CM} ($= C_m$) - (Fossen and Perez (2009)).

$$F_{Cv}(\theta_C) = \frac{1}{2} \rho_{water} L_{PP} T C_{CY}(\theta_C) U_C^2 \quad (13)$$

$$M_{Cz}(\theta_C) = \frac{1}{2} \rho_{water} L_{PP}^2 T C_{CM}(\theta_C) U_C^2 \quad (14)$$

4.3 Mean Drift Forces

The mean drift forces are computed considering both sea and swell conditions and combined as wave loads acting at the ship. The longitudinal and transversal forces and yaw moment are computed using Eqs. (13), (14) and (15), with $S_{\zeta}(\omega, T_P, H_S)$ representing the standard Jonswap spectrum; $\bar{F}_x(\omega, \theta_O)$, $\bar{F}_y(\omega, \theta_O)$ and $\bar{M}_z(\omega, \theta_O)$, the RAOs (Response Amplitude Operators) of the longitudinal and transverse forces and yaw moment and θ_O , the resulting incidence angle.

$$F_{Ox}(\theta_O) = 2 \int_0^{\infty} S_{\zeta}(\omega, T_P, H_S) |\bar{F}_x(\omega, \theta_O)| d\omega \quad (15)$$

$$F_{Oy}(\theta_O) = 2 \int_0^{\infty} S_{\zeta}(\omega, T_P, H_S) |\bar{F}_y(\omega, \theta_O)| d\omega \quad (16)$$

$$M_{Oz}(\theta_O) = 2 \int_0^{\infty} S_{\zeta}(\omega, T_P, H_S) |\bar{M}_z(\omega, \theta_O)| d\omega \quad (17)$$

The RAOs are computed using the higher order method of the WAMIT® potential flow solver taking into account for discretization angles between 0° (stern) and 180° (bow), as the hull is symmetrical and there is no interaction with the FPSO. The mean drift coefficients shown in Fig. 14.

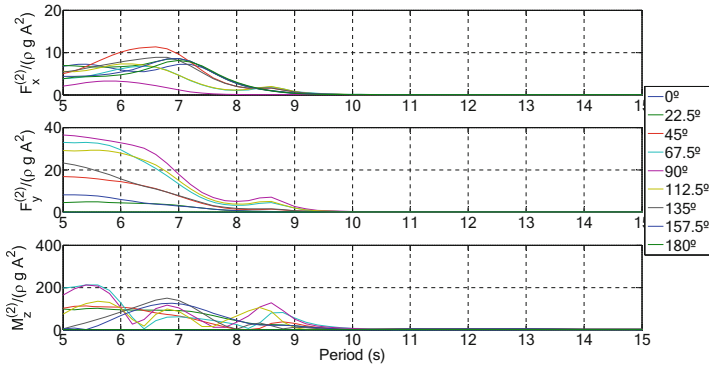


Fig. 14. Mean drift force coefficients computed using WAMIT Potential Flow code.

4.4 Wave Drift-Damping Forces

The wave drift damping forces are computed through Eqs. (16), (17) and (18) based on Aranha’s approximation (Aranha (1994)).

$$F_{WDDu}(\theta_O) = 2 \int_0^\infty S_\zeta(\omega, T_P, H_S) \frac{\omega}{g} \left[\left(\omega \frac{\partial \bar{F}_x}{\partial \omega} + 4\bar{F}_x \right) \cos \theta_O - 2 \frac{\partial \bar{F}_x}{\partial \theta_O} \sin \theta_O \right] d\omega \quad (18)$$

$$F_{WDDv}(\theta_O) = 2 \int_0^\infty S_\zeta(\omega, T_P, H_S) \frac{\omega}{g} \left[\left(\omega \frac{\partial \bar{F}_y}{\partial \omega} + 4\bar{F}_y \right) \cos \theta_O - 2 \frac{\partial \bar{F}_y}{\partial \theta_O} \sin \theta_O \right] d\omega \quad (19)$$

$$M_{WDDz}(\theta_O) = 2 \int_0^\infty S_\zeta(\omega, T_P, H_S) \frac{\omega}{g} \left[\left(\omega \frac{\partial \bar{M}_z}{\partial \omega} + 4\bar{M}_z \right) \cos \theta_O - 2 \frac{\partial \bar{M}_z}{\partial \theta_O} \sin \theta_O \right] d\omega \quad (20)$$

5 PSV Monitored Data

The AIS/AIS-Sat data were obtained for four different PSVs, however, as the vessel Bram Bahia had more information available (10,279 records), it was selected for the study. It should be noted that the ship’s data information is not equally distributed in time therefore the data has to be resampled in the simulations, besides the removal of incorrect/inconsistent data. The monitored positions of the vessels are illustrated in Fig. 15, all vessels operating near the Brazilian coastline in Campos and Santos Basins.

The breakdown of ships’ speed is a key aspect to identify the maximum expected efficiency improvement therefore the data was post-processed and segregated in six different speed ranges, as shown in Fig. 16. The data records show that the vessels’ speed profile corresponds to low speed (<3 knots), which may be explained by the large time spent on anchorage, waiting to begin DP operations and in DP mode. This fact is particularly interesting for the study of hybrid power generation since diesel engines have the worst fuel consumption performance when working far from the rated speed.

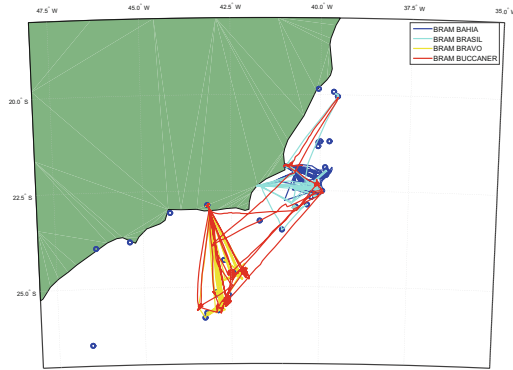


Fig. 15. Tracks of the monitored vessels.

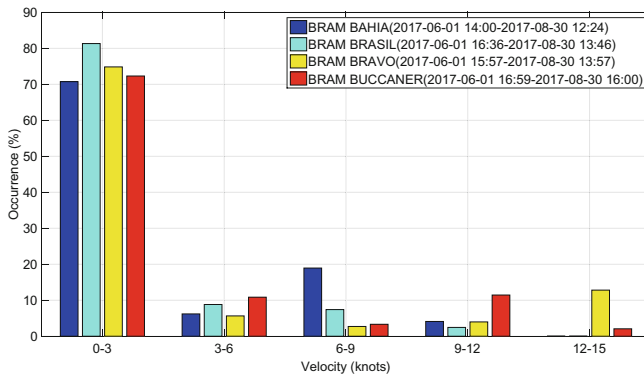


Fig. 16. Velocity distribution for the monitored vessels.

The vessel operational profile was split into five different conditions and for each one a specific approach was applied to provide the required thrust and therefore obtain the generator set loads and consumption. The characteristics of the five different states are:

- 1) Waiting for DP operation: Closer than 750 m of an oil platform, ship speed above 1,0 knot and no DP2 requirement;
- 2) Operating in DP mode: Quasi-static balance model at close proximity to the platform, with speed below 1.0 knot and DP2 requirement;
- 3) Sailing – Resistance assessment for speeds higher than 1.0 knots, estimated by Holtrop formulation, for calm water conditions and strip theory, for added resistance;
- 4) Anchored at port – Emergency generator plus one single engine;
- 5) Cargo Loading/Unloading – Only the emergency generator.

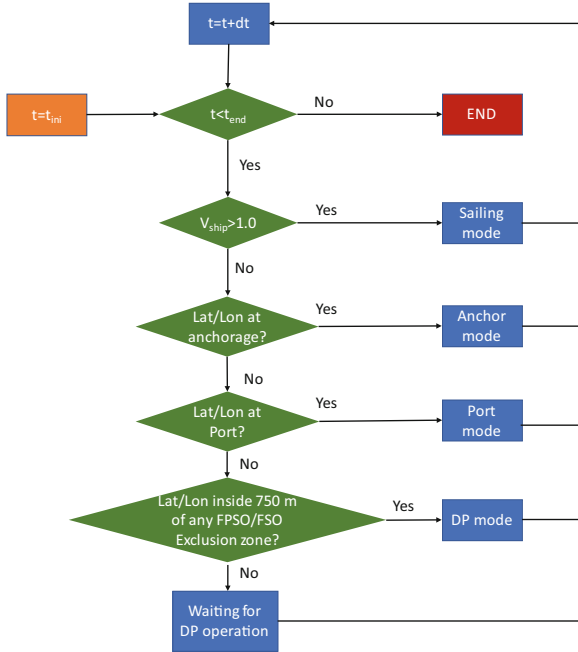


Fig. 17. Algorithm structure to identify vessel status during the simulations.

The algorithm applied to identify the vessel status is illustrated in Fig. 17, the main difficulty was to identify the waiting for DP operation condition, as this status is only roughly characterized.

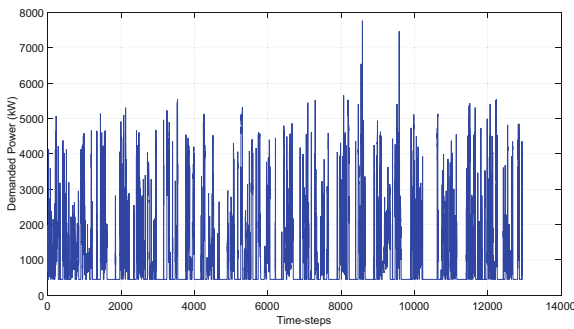


Fig. 18. Total required power during the Bram Bahia simulation.

6 Numerical Results

6.1 PSV Performance Simulation

The performance simulation of Bram Bahia was performed considering the previously described status. The demanded power timeline during the time-steps can be seen in Fig. 18, where large variations can be observed, which are mostly related to the sailing/navigating conditions with only two occasions in which the maximum available power was almost reached.

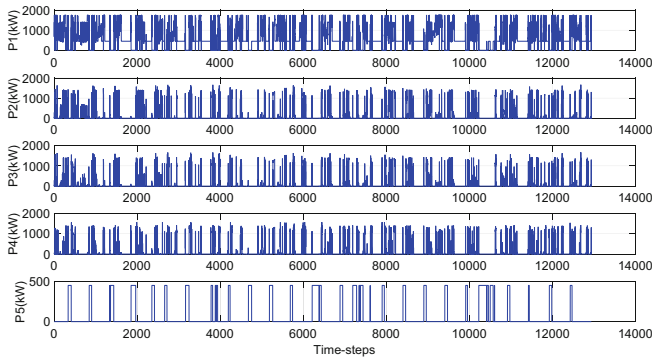


Fig. 19. Engine loads distribution for the several PSV engines.

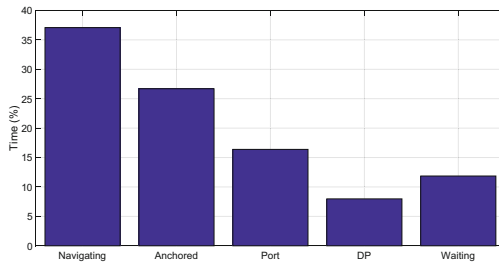


Fig. 20. Time distribution for the several vessel operational modes for Bram Bahia.

The engine loads timeline distribution is given in Fig. 19, where it can be seen that engine number 5 (P5) has a smaller maximum power compared to the others, its optimum SFOC being achieved under a smaller load condition, which could be advantageous if integrated with other engines for achieving the best compromise on fuel consumption.

The ship’s operational profile was established based on the total time for each operational mode as summarized in Fig. 20, where it can be seen that for almost 35% of the time the vessel is navigating while, for about 27% of the time, the vessel is

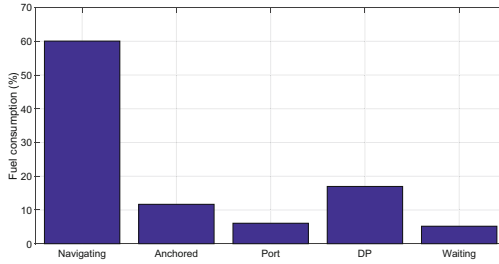


Fig. 21. Fuel consumption for the several operational modes for Bram Bahia.

anchored. The port, DP operation and waiting time percentages complete the operational profile.

The fuel consumption breakdown for each operation mode can be seen in Fig. 21, where it can be verified that the navigating condition represents almost 60% of the total fuel consumption and is appreciably higher than the other ones. It clearly shows the relevance of the high loads on the engine-generator sets used for navigation. On the other hand, the DP mode is responsible for about 18% of the total fuel consumption although corresponding only to 7% of the operational time.

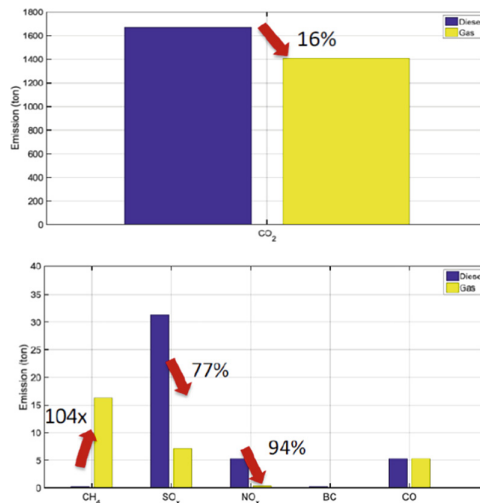


Fig. 22. Total CO₂, CH₄, SO_x, NO_x, BC and CO emissions from Bram Bahia.

The total CO₂ and other gases emissions for diesel engine and dual-fuel engine (natural gas mode) operation are illustrated in Fig. 22. It is clearly observed that operating on natural gas reduces CO₂ emissions to about 16%, SO_x in 77% and NO_x in 94%. By including a methane slip condition in the simulations, it is noted that the CH₄ emissions increase 104 times, its emission effect in the atmosphere being particularly severe and requiring a careful assessment of the power system design.

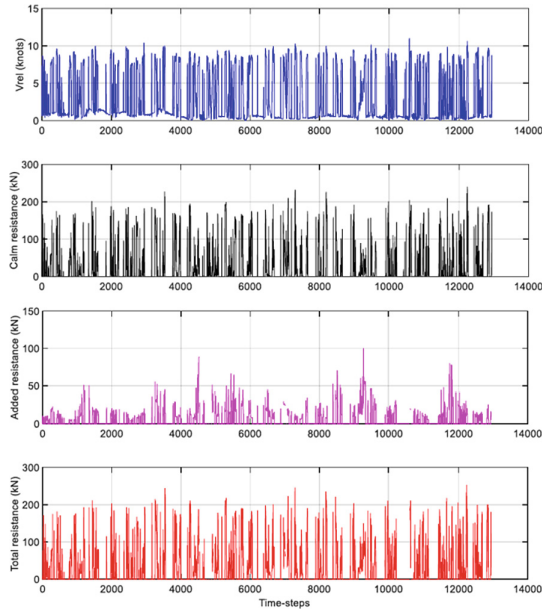


Fig. 23. Relative ship speed, calm, added and total resistance from Bram Bahia simulation.

The simulation regarding the sailing conditions resulted in the total resistance timeline distribution shown in Fig. 23, including calm and added resistance components as well as the relative ship speed (with current correction). It can be observed that there is a large variation in speed, which is directly correlated to the calm water resistance. On the other hand, the added resistance component depends strongly on sea state conditions, therefore it has a weaker correlation with speed, even though still significant.

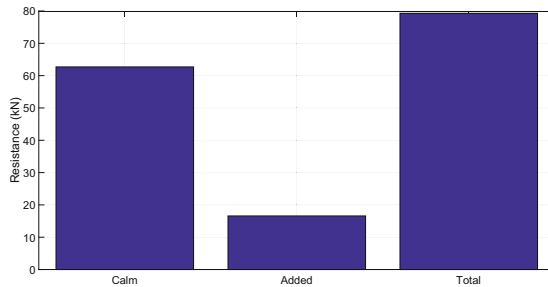


Fig. 24. Ship resistance breakdown for Bram Bahia.

The mean ship resistance breakdown for the previous ship speed distribution is given in Fig. 24, where the mean calm water resistance corresponds to about 63 kN,

while the mean added resistance is about 17 kN. It is interesting to note that the added resistance component represents about 27% of the calm water resistance, appreciably higher when compared to conventional merchant ship patterns in Brazil (~12%).

7 Conclusions

A simulator for PSV operations was developed taking into account ship particulars and available data of several equipment provided by manufacturers. The ship operational profile was established based on typical operation patterns and considering the Brazilian scenario of several oil platforms, main ports and anchorage regions.

The methodology applied consisted of retrieving the ship data on available AIS and AIS-Sat data from the internet and build a robust database with a specific script for post-processing the information. An algorithm was developed to automatically identify the ship status according to speed, latitude and longitude that, together with the environmental conditions database (current, wind and wave), made possible to generate a timeline of necessary information to simulate the operational profile of the ship.

Several numerical procedures were implemented and integrated. These include procedures for estimating the environmental (wind, current and waves) loads, the ship resistance (calm water and added resistance) components as well as for defining the thrust and power requirements. The procedure for determining the requirements of the tunnel and azimuth thrusters is based on a quasi-static approach applied at each time step and an optimization algorithm of thrust allocation for minimizing the ship's required power. Furthermore, an additional algorithm was implemented for optimizing the load distribution among the generator-engine sets for maximum ship energy efficiency (less fuel consumption).

The simulation of Bram Bahia showed that the main fuel consumption occurs during the navigation (~60%), this condition corresponding to only 35% of the total time. On the other hand, although associated with only 7% of the time, the DP operation mode is responsible for almost 18% of the fuel consumption; the anchored and port operation contributions being particularly small as the electric loads are minimal. Finally, the simulations showed clearly the potential of reducing CO₂ emissions with dual-fuel engines with additional reduction of SOX and NOX emissions, although care must be taken with the possibility of methane slip.

References

- Aranha, J.A.: A formula for wave damping in the drift of a floating body. *J. Fluid Mech.* **275**, 147–155 (1994)
- Blendermann, W.: Parameter identification of wind loads on ships. *J. Wind Eng. Ind. Aerodyn.* **51**, 339–351 (1994)
- Carlton, J.: *Marine Propellers and Propulsion*. Butterworth-Heinemann Ltd., Oxford (1994)
- Fossen, T.I., Perez, T.: Kalman Filtering for positioning and heading control of ships and offshore rigs: estimating the effects of waves, wind and current. *IEEE Control Syst. Mag.* **29**, 32–46 (2009)

- HYCOM. Hybrid Coordinate Ocean Model (2017). <https://www.hycom.org/>. Accessed 05 Apr 2017
- IPCC 2013. Climate Change 2013: The Physical Science Basis, Contribution of Working Group I to the Fifth Assessment Report of the Intergovernmental Panel on Climate Change [Stocker, T.F., Qin, D., Plattner, K., Tignor, M., Allen, S.K., Boschung, J., Nauels, A., Xia, Y., Bex, V., Midgley, P.M. (eds.)] 1535 p. Cambridge University Press, Cambridge (2013)
- Kjølleberg, J.: Weather Routing of Supply Vessels in the North Sea. Master Thesis, Department of Marine Technology, Norwegian University of Science and Technology – NTNU, Trondheim (2015)
- Rolls Royce. Propulsion systems for optimal operations under all conditions – Control the Power (2014). <https://www.rolls-royce.com/~media/Files/R/Rolls-Royce/documents/marine-product-finder/propulsion-brochure.pdf>. Accessed 30 June 2017
- Siemens. IEC Squirrel-Cage Motors (2012). https://w3.siemens.com.br/drives/br/pt/motores/motores-bt/motores-abnt-ate-3151/Documents/Catalogo_de_Motores_IEC_D81.1_-_2008.pdf. Accessed 12 Aug 2017
- Sternersen, D., Thonstad, O.: GHG and NOX emissions from gas fuel engine. Report OC2017 F-108, SINTEF Ocean AS Maritim (2017)
- Vasqués, C.A.M.: A methodology to select the electric propulsion system for Platform Supply Vessels (PSV). Master Thesis, Escola Politécnica, University of São Paulo (2014). (in Portuguese)